5-1-2024

Targeting dendritic cell dysfunction to circumvent anti-PD1 resistance in head and neck cancer

Shin Saito
Dana-Farber Cancer Institute
Michihisa Kono
Dana-Farber Cancer Institute
Hoang C B Nguyen
Brigham and Women's Hospital
Ann Marie Egloff
Dana-Farber Cancer Institute
Cameron Messier
Dana-Farber Cancer Institute

See next page for additional authors

Targeting Dendritic Cell Dysfunction to Circumvent Anti-PD1 Resistance in Head and Neck Cancer

Shin Saito[1], Michihisa Kono[1], Hoang C.B. Nguyen[2], Ann Marie Egloff[1,2], Cameron Messier[1,3], Patrick Lizotte[1,3], Cloud Paweletz[1,3], Douglas Adkins[4,5], and Ravindra Uppaluri[1,2]

ABSTRACT

Purpose: Neoadjuvant anti-PD1 (aPD1) therapies are being explored in surgically resectable head and neck squamous cell carcinoma (HNSCC). Encouraging responses have been observed, but further insights into the mechanisms underlying resistance and approaches to improve responses are needed.

Experimental Design: We integrated data from syngeneic mouse oral carcinoma (MOC) models and neoadjuvant pembrolizumab HNSCC patient tumor RNA-sequencing data to explore the mechanism of aPD1 resistance. Tumors and tumor-draining lymph nodes (DLN) from MOC models were analyzed for antigen-specific priming. CCL5 expression was enforced in an aPD1-resistant model.

Results: An aPD1-resistant mouse model showed poor priming in the tumor DLN due to type 1 conventional dendritic cell (cDC1) dysfunction, which correlated with exhausted and poorly responsive antigen-specific T cells. Tumor microenvironment analysis also showed decreased cDC1 in aPD1-resistant tumors compared with sensitive tumors. Following neoadjuvant aPD1 therapy, pathologic responses in patients also positively correlated with baseline transcriptomic cDC1 signatures. In an aPD1-resistant model, intratumoral cDC1 vaccine was sufficient to restore aPD1 response by enhancing T-cell infiltration and increasing antigen-specific responses with improved tumor control. Mechanistically, CCL5 expression significantly correlated with neoadjuvant aPD1 response and enforced expression of CCL5 in an aPD1-resistant model, enhanced cDC1 tumor infiltration, restored antigen-specific responses, and recovered sensitivity to aPD1 treatment.

Conclusions: These data highlight the contribution of tumor-infiltrating cDC1 in HNSCC aPD1 response and approaches to enhance cDC1 infiltration and function that may circumvent aPD1 resistance in patients with HNSCC.

Introduction

Head and neck squamous cell carcinomas (HNSCC) are the seventh most common cancer worldwide with over 800,000 new cases per year (1). For HPV-negative locally advanced HNSCC, primary surgery- or radiotherapy-based regimens have been the main treatment modalities for decades with modest improvement in 5-year survival rates (2). FDA approvals of anti-PD1 (aPD1) mAb for recurrent/metastatic HNSCC have changed the standard of care for these patients. However, tumor response rates are limited to 15% to 20% (3, 4–6), and further approaches to enhance efficacy are needed.

Diverse immune checkpoint blockade (ICB) resistance mechanisms, including tumor-intrinsic and extrinsic factors, have been reported with responding tumors manifesting several common features (7, 8). The baseline tumor microenvironment (TME), classified as either hot, cold, immune excluded, or immune suppressed (9), is directly linked to ICB response and provides a conceptual framework for enhancing therapeutic efficacy. "Hot" or "immune-inflamed" tumors have been shown to respond favorably to ICB treatment because of pre-existing infiltrating cytotoxic $CD8^+$ T cells and M1 macrophages. By contrast, increased regulatory $CD4^+$ T cells, myeloid-derived suppressor cells, and M2 macrophages in the TME are associated with poor tumor response. Recent studies have shown that dendritic cells (DC), especially conventional type 1 DC (cDC1) positively correlate with survival (10) as well as ICB response in melanoma (11). This is in line with the findings that cDC1 are a key cross-presenting cell for antitumor $CD8^+$ T cells and express T-cell–attracting chemokines (12). Outcomes for patients with HNSCC treated with standard-of-care therapies correlate with cDC1 infiltration (13), and furthermore, preclinical HNSCC models show the importance of cDC1 for aPD1 response (14). However, whether cDC1 infiltration correlates with ICB response in human patients with HNSCC has not yet been defined. Furthermore, the underlying mechanism(s) of how cDC1 infiltration differs between distinct TME immune types is not fully understood.

Here, we focus on defining the contribution of DC to neoadjuvant aPD1 response in HNSCC. Analysis of pretreatment biopsies from a neoadjuvant aPD1 clinical trial, where previously untreated patients have an unperturbed immune system, allowed us to examine associations of tumor-infiltrating cDC1 with the extent of tumor response. Extending this work to a mouse oral carcinoma model with differential response to aPD1 treatment, we further aimed to reveal the mechanism behind cDC1 recruitment into the tumor.

Materials and Methods

Cell lines/mouse studies

Mouse oral squamous cell carcinoma (MOC) cell lines, MOC22 (RRID:CVCL_ZD36), MOC2 (RRID:CVCL_ZD33), MOC1P (= MOC1 parental, RRID:CVCL_ZD32), and MOC1esc1 were generated as

[1]Department of Medical Oncology, Dana-Farber Cancer Institute, Boston, Massachusetts. [2]Department of Surgery/Otolaryngology, Brigham and Women's Hospital, Boston, Massachusetts. [3]Belfer Center for Applied Cancer Science, Dana-Farber Cancer Institute, Boston, Massachusetts. [4]Alvin J. Siteman Cancer Center, Washington University School of Medicine, St. Louis, Missouri. [5]Department of Medicine/Medical Oncology, Washington University School of Medicine, St. Louis, Missouri.

S. Saito and M. Kono contributed equally as co-authors of this article.

Corresponding Author: Ravindra Uppaluri, Dana-Farber/Brigham and Women's Cancer Center, 450 Brookline Avenue, Boston, MA 02215. E-mail: ravindra_uppaluri@dfci.harvard.edu

Clin Cancer Res 2024;30:1934–44

doi: 10.1158/1078-0432.CCR-23-3477

Translational Relevance

Understanding anti-PD1 (aPD1) resistance mechanisms and means to bypass these are a key obstacle to broaden benefit to a wider population of patients with cancer. Herein, using complementary data from neoadjuvant aPD1-treated patients with HNSCC and mouse models, we identified dendritic cell (DC) paucity and their functional defects correlating with a lack of response. A DC vaccine loaded with endogenous tumor antigens was sufficient to restore aPD1 sensitivity in a mouse model. CCL5 expression correlated with aPD1 response in the neoadjuvant HNSCC cohort. Enforced expression of this chemokine remodeled the tumor microenvironment, restored aPD1 sensitivity, and improved antigen-specific T-cell responses. These results identify a cDC1 contribution to HNSCC aPD1 responses and a mechanistic approach to enhancing DC/T-cell function to circumvent resistance.

previously described (15, 16). All MOC cell lines were cultured in MOC medium (IMDM (Gibco, No. 12440061), Ham's F12 nutrient mixture (Gibco, No. 11765047), 5% heat-inactivated FBS (Sigma, No. F2442), 100 U/mL penicillin–streptomycin (Thermo Fisher Scientific, No. BW17603E), 5-ng/mL EGF (Thermo Fisher Scientific, No. 01107MI), 400 ng/mL hydrocortisone (Sigma, No. H0888), and 5 μg/mL insulin (Sigma, No. I0516) in a 37°C incubator. Cell lines were routinely tested for *Mycoplasma* and underwent short tandem repeat cell line authentication at the DFCI within 6 months of use. Cell lines were passaged no more than 10 times after thawing from original stocks. Female wild-type C57BL/6 mice (Taconic Biosciences, 6 to 9 weeks old) were housed in a specific pathogen-free animal facility. All animal studies were conducted in compliance with regulations of the institutional animal care and use committee of Dana-Farber Cancer Institute.

Transduction of MOC1P, MOC1esc1, and MOC2 cell lines

Ovalbumin (OVA)-derived SIINFEKL-expressing MOC1P (MOC1P-ova) was a gift from Dr. Clint Allen (NIH). SIINFEKL-expressing MOC1esc1 (MOC1esc1-ova) was generated using mKATE-2–SIINFEKL retrovirus (from Dr. Clint Allen, NIH). mKATE-2–SIINFEKL retrovirus was produced in 293T cells (RRID: CVCL_0063) by cotransfection of gag/pol and VSV-G vectors (RRID:Addgene_138479) using Lipofectamine 3000 (Thermo Fisher Scientific) and was used to transduce MOC1esc1. Transduced MOC1P-ova and MOC1esc1-ova were sorted for mKate2-positive cells. To generate CCL5-expressing MOC1esc1 and MOC2, a CCL5 (NM_013653) gBlock (IDTDNA) was cloned into a pLV vector-expressing mKate2 using HiFi DNA assembly (New England BioLabs). Lentivirus was produced in 293T cells by co-transfection of delta8.9 and VSV-G vectors. Virus was concentrated by Lenti-X Concentrator (Takara Bio), resuspended in MOC medium, and transduced into MOC1esc1 and MOC2. Cells were sorted for mKate2 positivity with expression routinely monitored before each experiment. MOC1esc1-expressing full-length OVA (MOC1esc1-OVA) was generated by using OVA-expressing pLX311 vector and selecting with blasticidin.

Cancer cell line inoculation, tumor models, and *in vivo* antibody treatment

MOC cell lines were cultured and after harvest and washing (>90% viability), were resuspended in PBS with 33% volume BME (Basement Membrane Extract, Thermo Fisher Scientific, No. 353200502) and kept on ice until inoculation. Tumor cell line inoculation ($1–2\times10^6$) was performed either subcutaneously in the flank, or submucosally in the buccal mucosa. Tumor sizes were measured two to three times per week, and tumor volume was calculated as $(\text{length}\times\text{width}^2)/2$. ICB treatment was performed by intraperitoneal injections of either aPD1 antibody (BioXcell, No. BE0146250, 250 μg per mouse per injection) or isotype control antibody (BioXcell, No. BE0089, 250 μg per mouse per injection) on days 3, 6, and 9 after tumor implantation.

ELISA assays

Quantikine ELISA Mouse IFNγ Immunoassays (R&D Systems) were performed for IFNγ quantification, and mouse CCL5 ELISA Kit (KE10017, Proteintech) was used for CCL5 quantification according to the manufacturer's instructions. For IFNγ assays, cells were treated with PMA (2 μg/mL) and ionomycin (0.1 μg/mL) for positive control.

Mouse IFNγ enzyme-linked immunospot assays

Enzyme-linked immunospot (ELISPOT) was performed using the mouse IFNγ single-color ELISPOT kit (ImmunoSpot by CTL). MOC1esc1-draining lymph nodes (DLN) and spleens from mice treated with isotype control, aPD1, DC vaccine, or combination were assayed for reactivity to neoantigen peptides. Lymph nodes and spleens were gently disaggregated with frosted glass slides and filtered after RBC lysis. After washing once, cells were counted, and a total of 5.0×10^5 DLN cells/splenocytes were suspended in 100 μL of CTL serum-free medium and stimulated with 1 μmol/L of peptides (mYipf1; VALATFVTI, p15e; KSPWFTTL Peptide 2.0) in each well of a murine IFNγ Immunospot System (CTL) for 24 hours at 37°C. PMA (2 μg/mL) and ionomycin (0.1 μg/mL) stimulation was used for positive control. IFNγ spots/well were then detected and quantified by a plate reader.

Tumor dissociation and flow-cytometry staining

Tumors were harvested, mechanically dissociated, and digested with DNase (100 U/mL, Roche No. 4536282001) and collagenase type IV (Life Technologies No. 17104019) at 37°C for 45 to 60 minutes. Tumors were further dissociated through an 18-g needle or with vigorous pipetting. After filtering through a 40-μm strainer, cells were washed and resuspended for staining. The tumor DLN was defined as the ipsilateral inguinal lymph node for flank tumors. For oral tumors, a single dominant ipsilateral submandibular lymph node, adjacent to the submandibular gland was harvested. Lymph nodes were gently disaggregated with frosted glass slides in RPMI and filtered through a 40-μm strainer to generate single cells and were washed and resuspended for staining.

After Zombie Aqua (BioLegend) viability dye staining and Fc-block, fluorophore-labeled antibodies were directly added to each sample and incubated at 4°C for 25 to 30 minutes. For ova-SIINFEKL dextramer staining (Immudex, JD02163), samples were treated with dasatinib (final concentration 50 nmol/L) and incubated at 37°C for 30 minutes before adding 5 μL of dextramer and incubating at room temperature for 15 minutes.

Samples were run on a MACS-Quant 10 (Miltenyl) or LSR Fortessa (BD Biosciences), and data were analyzed with FlowJo v10 (BD Biosciences, RRID:SCR_008520). The following fluorescence-conjugated antibodies were used (all from BioLegend): mouse CD45.2 (104), mouse CD3ε (145–2c11), mouse CD4 (RM4–4), mouse CD8α (53–6.7), mouse CD279 (PD-1, 29F.1A12m), mouse CD25 (PC61), mouse NK1.1 (PK136), mouse CD19 (6D5), mouse F4/80 (BM8), mouse I-A/I-E (M5/114.15.2), mouse CD11c (N418), mouse Xcr1 (ZET), mouse Sirpα (p84), mouse Tim3 (RMT3–23), mouse Lag3

(C9B7W), mouse Ly-6c (HK1.4), mouse/human KLRG1 (2F1/KLRG1), mouse CD40 (3/23), mouse CD80 (16–10A1), and mouse CD86 (GL-1).

Tumor-infiltrating lymphocyte culture

For functional analysis of tumor-infiltrating lymphocyte (TIL), tumors were harvested in aseptic condition and cut into 1- to 2-mm cube pieces. Individual tumor fragments were cultured in T-cell medium (RPMI-1640; Gibco, No. 11875–093), 5% heat-inactivated FBS (Sigma, No. F2442), 100 U/mL penicillin–streptomycin (Thermo Fisher Scientific, No. BW17603E), 1 mmol/L sodium pyruvate (Sigma, No. 8636), 50 mmol/L BME, 2 mmol/L L-glutamine (Gibco, No. 25030–081), 20 mmol/L HEPES (Gibco, No. 15630080) supplemented with human IL2 (100 U/mL, Roche TECIN, No. Ro 23–6019) for 48 hours in a 24-well plate. Cells were collected and filtered through a 40-μm strainer. After washing with PBS, dead cell removal was performed using magnetic beads (Miltenyi Biotech, No. 130–090–101) and then used for functional analysis.

Quantitative PCR

RNA was extracted from MOC1esc1 tumors (day 14) and converted to cDNA using the RNA to cDNA high-capacity kit (Thermo Fisher Scientific). Mouse Xcr1 gene-specific primers (IDT DNA) were validated and used in SYBR green quantitative PCR (qPCR). Relative quantification by the $\Delta\Delta C_t$ method was used with *Gapdh* expression as the endogenous control. Primer sequences were as follows: *Gapdh* 5′-CCGGTGCTGAGTATGTCGTG-3′, *Gapdh* 3′-GTGACGGTGGGTCTTCTGAC-5′, *Xcr1* 5′-AGAGACACCGAACAGTCAGGCT-3′, *Xcr1* 3′-TGTCCAGTTGCTGAAGGCTCTC-5′. qPCR was assayed on a QuantStudio 3 (Applied Biosystems) and analyzed with Design and Analysis Software (v. 2.6).

Mouse *in vivo* tumor RNA-sequencing data analysis

RNA-sequencing (RNA-seq) of MOC tumors was previously described (16). *In vivo* expression was evaluated in normalized bulk RNA-seq data from MOC22 tumors harvested on day 17, and MOC1P and MOC1esc1 tumors harvested on day 14 after implantation.

Patient HNSCC tumor bulk RNA-seq

RNA-seq data from a neoadjuvant pembrolizumab HNSCC clinical trial (NCT02296684; ref. 17) were interrogated, and response to neoadjuvant aPD1 was classified on the basis of pathological tumor response (pTR) in surgical specimens with pTR-0 (<10% pathologic response); pTR-1 (10%–49% response); pTR-2 (≥50% response; ref. 17). pTR-0 patients were classified as nonresponders and pTR-1 and 2 as responders.

Patient HNSCC tumor single-cell RNA-seq

Single-cell RNA sequence (scRNA-seq) data were generated from a neoadjuvant HNSCC pembrolizumab clinical trial (18). Pathological response was categorized as described above. $CD45^+$ cells were sorted from pre- and posttreatment specimens from two responders and two nonresponder patients. Sample cell count and viability were assessed by trypan-blue dye exclusion (Sigma-Aldrich), and cell density was adjusted to analyze approximately 10,000 cells per sample. Sample processing for single-cell gene expression (scRNA-seq) was performed (Chromium Single Cell 3′ Library and Gel Bead Kit, 10x Genomics) following the manufacturer's recommendations. After Gel Bead-in-Emulsion reverse transcription (GEM-RT) reaction and clean-up, PCR amplification was performed to obtain cDNA for RNA-seq library generation according to the manufacturer's instructions. Quality controls for cDNA and sequencing libraries were performed using a Bioanalyzer High Sensitivity DNA Kit (Agilent). All libraries were uniquely indexed for multiplexed sequencing using the Illumina NextSeq 500 platform.

DC generation and vaccination

B16-FLT3 L cells (RRID: CVCL_IJ12, gift from G. Dranoff/U. von Andrian) were used to generate cDC1 as described (19). Briefly, B16-FLT3 L cells were cultured in DMEM supplemented with 10% FBS, and 1% penicillin–streptomycin and cells (2.0×10^6) were implanted subcutaneously into the flanks of wild-type C57BL/6 mice with splenocyte harvest on day 12. Spleens were gently disaggregated with frosted glass slides in 5 mL of DC medium [RPMI-1640 (Gibco, No. 11875–093), 10% FBS, 1% Pen/Strep, 1 mmol/L sodium pyruvate, 50 mmol/L BME]. After RBC lysis, DC were purified with Xcr1+ beads (Miltenyi Biotech No. 130–115–721) followed by stimulation with PolyI:C (20 μg/mL) and tumor antigen peptides [mYipf1; VALATFVTI, p15e; KSPWFTTL (Peptide 2.0), 20 μg/mL each)] for 4 hours. DC were collected and used for intratumoral vaccine (1.0×10^6 cells in PBS; 100 μL).

In vitro DC migration assay

Activated Xcr1+ DC (3×10^5 in 100 μL of DC medium) were placed in the upper well of Transwell plates (Costar, 5 μmol/L pore size, 6.5-mm insert) with 600 μL of MOC medium or culture supernatant from MOC1esc1 or MOC1esc1-CCL5 in the lower well and allowed to migrate at 37°C for 4 hours. Migrated cells were harvested and quantified by flow cytometry.

DC antigen presentation assay

Xcr1+ DC (3×10^4) were cocultured with magnetically isolated $CD8^+$ OT1 cells in the presence of ova short peptide (SIINFEKL), ova synthetic long peptide (KISQAVHAAHAEINEAGRESIINFEKLTEWT), MOC1esc1 cell lysate, or MOC1esc1-OVA (MOC1esc1-expressing full-length OVA) cell lysate for 48 hours and evaluated for IFNγ production by ELISA.

Statistical analysis

One-way ANOVA followed by Tukey's multiple comparison, unpaired Mann–Whitney tests, and two-way ANOVA tests were used for statistical comparisons as indicated in each figure using GraphPad Prism version 9 (RRID:SCR_002798). Significant differences of $P < 0.05$, 0.01, and 0.001 are shown as *, **, and ***, respectively.

Data availability

Mouse RNA-seq has been previously deposited (NCBI GEO; GSE153383). Human scRNA-seq data are available through the dbGaP accession phs 002864.v1.p1 (https://www.ncbi.nlm.nih.gov/projects/gap/cgi-bin/study.cgi?study_id=phs002864.v1.p1). MOC cell lines are available from Kerafast.

Results

aPD1-resistant model shows reduced priming due to cDC1 dysfunction in tumor DLN

To investigate the mechanisms underlying aPD1 resistance, we used an isogenic paired MOC1P and MOC1esc1 model that showed response or resistance to aPD1 therapy, respectively (16). To examine antigen-specific responses, we used OVA-derived SIINFEKL model antigen-expressing MOC1P and MOC1esc1 lines (MOC1P-ova and MOC1esc1-ova). Of note, MOC1P-ova remained aPD1-sensitive (**Fig. 1A**), and MOC1esc1-ova remained aPD1-resistant (data not shown). To confirm that tumor DLN are critical for aPD1 response in

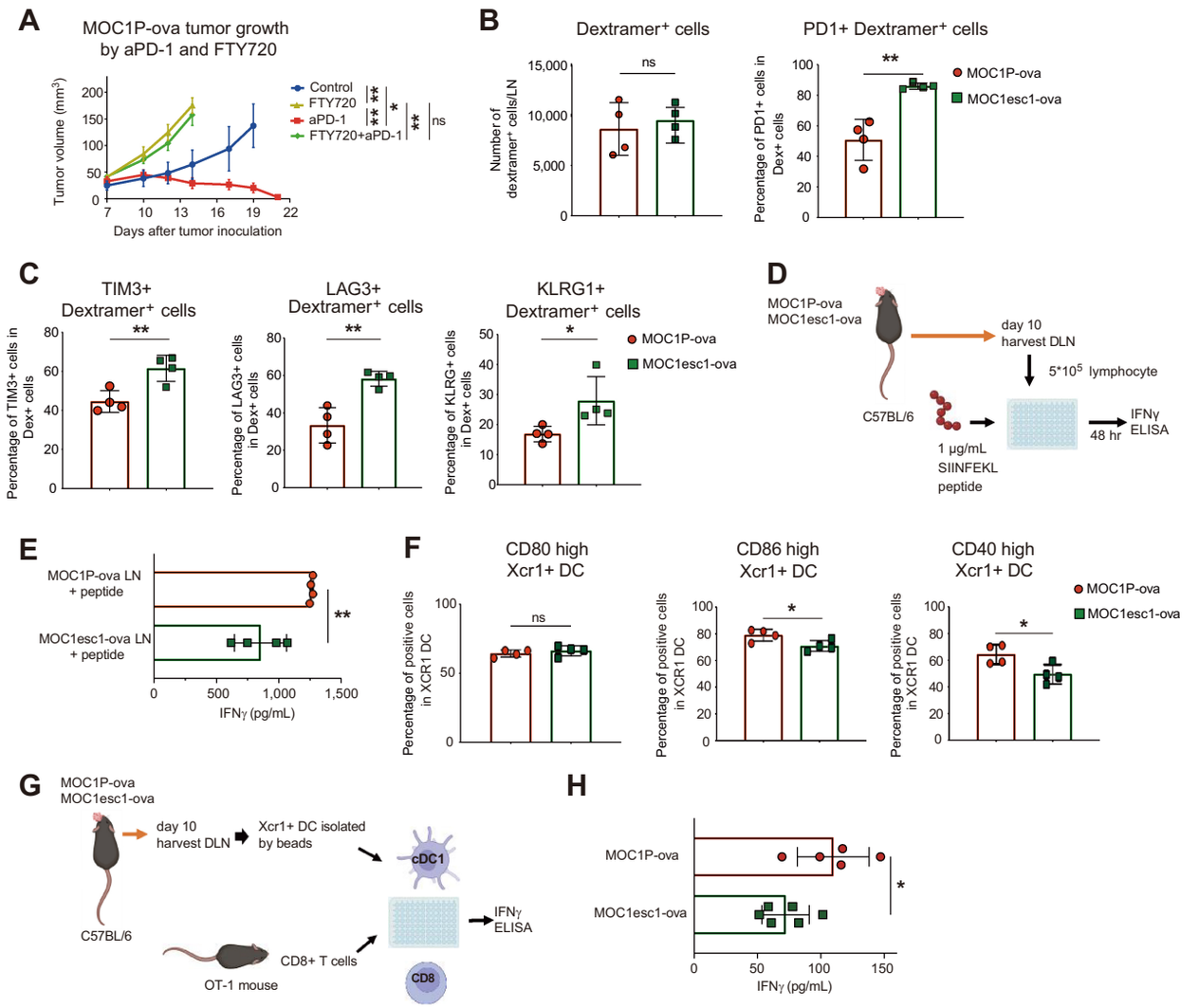

Figure 1.

aPD1-resistant model shows reduced priming due to cDC1 dysfunction in tumor-draining lymph nodes (DLN). **A,** *In vivo* tumor growth of MOC1P-ova after treatment with aPD1 (250 µg IP on days 3, 6, and 9) or FTY720 (10 µg IP daily from one day before inoculation). ($n = 4$ tumors for each group). **B** and **C,** Flow-cytometric analysis of MOC1P-ova/MOC1esc1-ova DLN on day 10 after inoculation ($n = 4$ for each group, representative data of two independent experiments). **D,** Representation of experiment in **E**. **E,** Tumor DLN from orthotopically inoculated MOC1P-ova/esc1-ova–bearing mice were harvested on day 10 and stimulated with SIINFEKL peptide for 48 hours to assess IFNγ production by ELISA ($n = 4$ for each group, representative data of two independent experiments). **F,** Flow-cytometric analysis of costimulatory markers on Xcr1$^+$ DC in DLN of MOC1P-ova/MOC1esc1-ova harvested 10 days after tumor inoculation ($n = 4$ for each group, representative data of two independent experiments). **G,** Representation of experiment in **H**. **H,** Xcr1$^+$ DC magnetically isolated from DLN of MOC1P-ova/MOC1esc1-ova were cocultured with CD8$^+$ OT1 T cells to test priming ability evaluated by IFNγ ELISA ($n = 5$–6, representative data of two independent experiments). Data are plotted as mean ± SEM in **A** and individual data with mean ± SD in all other panels. Data were analyzed using two-way ANOVA with multiple comparison for **A** and Mann–Whitney *U* test to generate two-tailed *P* values in **B**, **C**, **E**, **F**, and **H**. (**D** and **G** were generated by using BioRender under granted license.) *, $P < 0.05$; **, $P < 0.01$; ns, not significant.

MOC1P, we treated orthotopic MOC1P-ova–bearing mice with FTY720, a sphingosine 1-phosphate (S1P) receptor agonist that inhibits lymph nodes cell egress. aPD1 sensitivity was abrogated with FTY720 treatment (**Fig. 1A**), confirming that tumor-reactive cells induced in the lymph nodes were responsible for aPD1 rejection. Although the number of dextramer-positive cells in the DLN did not differ (**Fig. 1B**), phenotypic analysis revealed that antigen-specific cells from MOC1esc1-ova bearing mice had increased expression of PD-1, TIM3, LAG3, and KLRG1 consistent with an exhausted state compared with MOC1P-ova (**Fig. 1B** and **C**). Also, consistent with this dysfunctional state, CD8$^+$ T cells isolated from MOC1esc1-ova DLN showed reduced IFNγ production upon peptide restimulation (**Fig. 1D** and **E**). As impaired priming is known to be one of the reasons exhausted T cells are induced (20), these data led us to hypothesize that MOC1esc1 had impaired priming in the lymph nodes, resulting in dysfunctional CD8$^+$ tumor-reactive T cells. To test this, we assessed MOC1esc1-ova and MOC1P-ova DLN for Xcr1$^+$ cDC1. Although the number of cDC1 did not differ (Supplementary Fig. S1A), costimulation markers found modest reduction in CD86 and CD40 expression in resistant tumor-bearing mice (**Fig. 1F**). Importantly, Xcr1+ cDC1

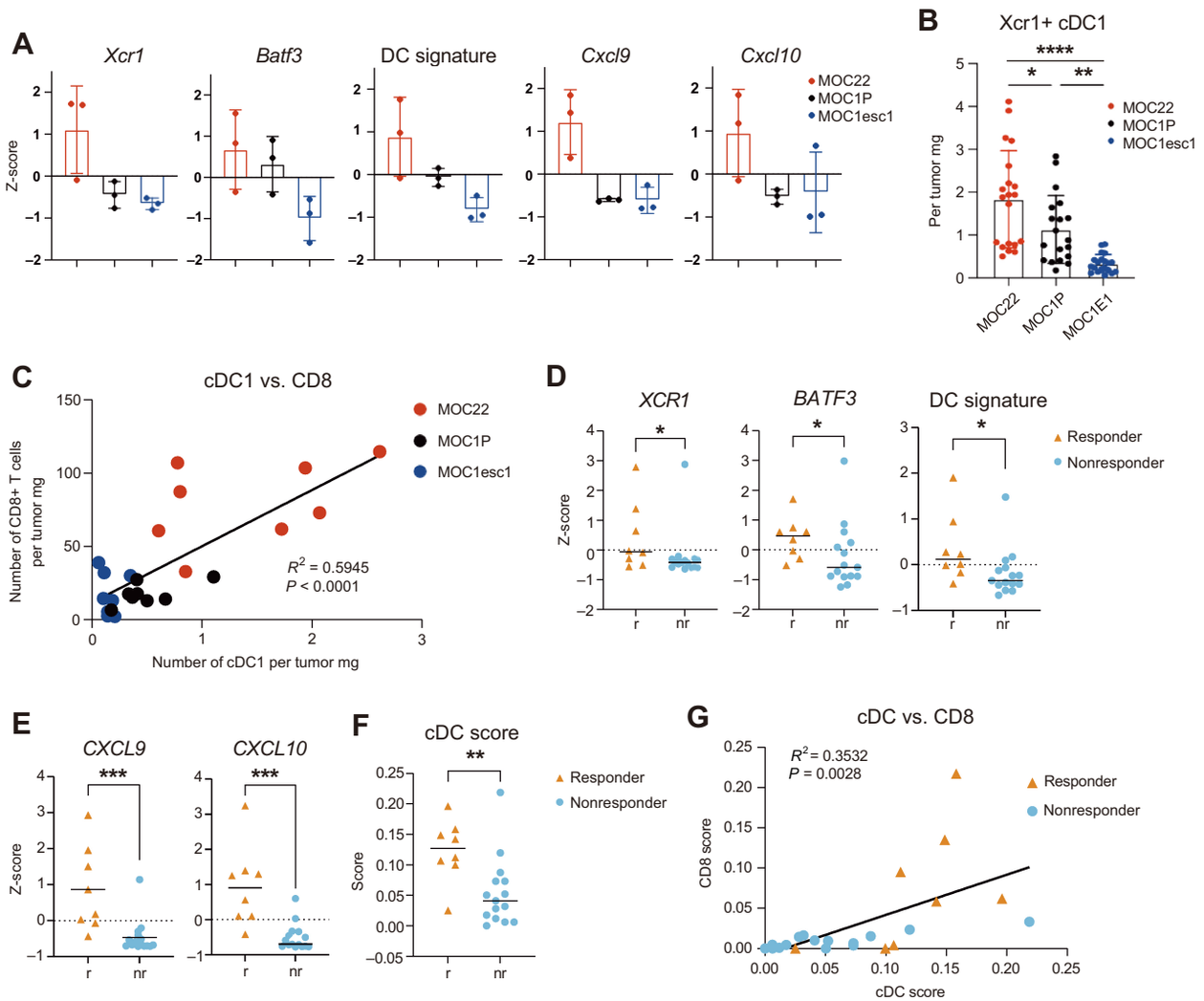

Figure 2.

aPD1 sensitivity is correlated with DC infiltration in mouse and human HNSCC. **A,** Bulk RNA-sequencing data from MOC22 tumors harvested on day 17, and MOC1P and MOC1-esc1 tumors harvested on day 14 after implantation are shown for indicated genes as z-score ($n = 3$ for each model). "DC signature" represents the average z-score of Batf3, Xcr1, Clnk, and Clec9a (10). **B,** Flow-cytometric data of Xcr1+ cDC1 from MOC22, MOC1P and MOC1esc1 tumors harvested on day 12 after inoculation (numbers are shown as cells per tumor mg, $n = 19$–20, pooled data from three independent experiments, gating strategies shown in Supplementary Fig. S2G). **C,** Correlation of cDC1 and CD8$^+$ T cells from flow-cytometric data in MOC22, MOC1P, and MOC1esc1 tumors harvested on day 12 after inoculation (numbers are shown as cells per tumor mg, $n = 8$, representative data from three independent experiments, gating strategies shown in Supplementary Fig. S2F and S2G). **D** and **E,** Bulk RNA-seq data of indicated genes in pretreatment tumor samples from patients who received subsequent aPD1 therapy shown as z-score ($n = 8$ responders and $n = 15$ nonresponders). "DC signature" represents the average z-score of BATF3, XCR1, CLNK, and CLEC9a (10). **F** and **G,** cDC and CD8 score calculated from a general cell type enrichment analysis webtool (23) using the same dataset as in **D**. Individual data with mean ± SD are plotted in **A** and **B,** and individual data with mean are plotted in **D**–**F**. Data were analyzed using the Mann–Whitney *U* test to generate two-tailed *P* values in **D**–**F** and Pearson correlation coefficient in **C** and **G** and one-way ANOVA followed by Tukey's multiple comparison for **B**. *, $P < 0.05$; **, $P < 0.01$; ***, $P < 0.001$; ****, $P < 0.0001$.

isolated from DLN of MOC1esc1-ova had significantly reduced capacity to prime OT-1 T cells (**Fig. 1G** and **H**). These data are consistent with reduced DLN functionality of Xcr1+ cDC1 leading to insufficient T-cell priming in this aPD1-resistant HNSCC mouse model.

aPD1 resistance is correlated with DC infiltration in patients with HNSCC and mouse models

As Xcr1+ cDC1 are known to capture antigens in the tumor and migrate into the DLN, we next examined the tumors themselves for any differences in DC populations. We compared bulk RNA-seq data between three models that show differential response to aPD1-MOC1P, MOC1esc1, and MOC22, which is a checkpoint inhibitor–sensitive model with complete aPD1 response (21). Interestingly, we saw a correlation of cDC1-related gene expression, namely Batf3 and Xcr1and response to aPD1 (**Fig. 2A**). Furthermore, a published cDC1 signature (10) also correlated with aPD1 sensitivity, with MOC22 showing the highest and MOC1esc1 the lowest expression (**Fig. 2A**; Supplementary Fig. S2A). *CXCL9/10*, which are chemokines known to be expressed by intratumoral DC (22), were also upregulated in

sensitive models (**Fig. 2A**). These findings were confirmed by qPCR from *in vivo* MOC cell line–generated tumors (Supplementary Fig. S2B). Flow-cytometric analysis of *in vivo* established tumors confirmed Xcr1+ cDC1 paucity in MOC1esc1 tumors compared with MOC1P and MOC22 (**Fig. 2B**), along with other immune populations such as $CD45^+$ cells and $CD3^+$ T cells (Supplementary Fig. S2D and S2E). Furthermore, cDC1 infiltration and CD8 infiltration showed significant correlations (**Fig. 2C**).

To extend these findings to human HNSCC, we analyzed treatment-naïve biopsy specimens from patients who received subsequent neoadjuvant pembrolizumab (NCT02296684). Transcriptomic analysis showed that patients with a pathological response to aPD1 showed higher DC-related gene expression compared with nonresponders at baseline, with significantly increased expression of *BATF3* and *XCR1* in responders ($P = 0.0337$ and 0.0477, respectively, **Fig. 2D**). Furthermore, a cDC1 signature (10) was also significantly elevated in the responder group ($P = 0.0159$, **Fig. 2D**; Supplementary Fig. S2C). *CXCL9/10* were also significantly upregulated in the responders ($P = 0.0003$ and 0.0002, respectively, **Fig. 2E**). A general cell type enrichment analysis webtool (23) showed similar results, with a significantly higher cDC score in responders ($P = 0.0080$, **Fig. 2F**) that was correlated with a CD8 score (**Fig. 2G**). Collectively, these data indicate that intratumoral cDC1 positively correlate with neoadjuvant aPD1 response in newly diagnosed human patients with HNSCC, similar to our mouse model.

Intratumoral $xcr1^+$ DC vaccine induces antigen-reactive T cells in the DLN and is sufficient to overcome aPD1 resistance in HNSCC mouse model

Given the cDC1 paucity in the TME and poor T-cell priming in the DLN of MOC1esc1, we investigated whether intratumoral delivery of an Xcr1+ cDC1 vaccine platform bearing endogenous tumor antigens would be sufficient to overcome aPD1 resistance. Xcr1+ cDC1 were isolated from B16-FLT3 L inoculated C57BL/6 mouse splenocytes (**Fig. 3A**). Representative surface markers and antigen presentation ability were confirmed by flow cytometry (Supplementary Fig. S3A and S3B) and an *in vivo* presentation assay (Supplementary Fig. S3C and S3D), respectively. Using these Xcr1+ cDC1, we first tested whether we could induce tumor antigen-specific T cells in the DLN of MOC1esc1. As a first step, we used an immunogenomic approach and identified the p15E (24) endogenous retrovirus-derived peptide and a neoantigen derived from a mutated Yipf1 allele (data not shown) as natural tumor antigens in MOC1P. Mice bearing MOC1esc1 tumors were treated intratumorally with a peptide-loaded Xcr1+ cDC1 vaccine. After three intratumoral cDC1 injections, we harvested DLN and spleen cells and analyzed antigen-specific reactivity. Compared with intratumoral PBS injection, antigen-reactive T cells increased in the DLN, showing that T-cell activation was enhanced through increased priming by intratumoral DC vaccination (**Fig. 3B**). Antigen reactivity in the spleen was also enhanced, showing a systemic effect of this treatment (**Fig. 3B**). Furthermore, given that Xcr1+ cDC1 are known to recruit $CD8^+$ T cells through expression of chemokines such as CXCL9/10, we examined the TME and DLN immune cell population after DC vaccine (**Fig. 3C** and **D**; Supplementary Fig. S3E and S3F). Xcr1+ cDC1 vaccine increased the numbers of total intratumoral $CD45^+$ immune cells and $CD3^+$ T cells (**Fig. 3C**). Total $CD8^+$ and $CD8^+PD1^+$ T cells also increased in the tumor (**Fig. 3C**). The number of $Xcr1^+$ cDC1 did not increase in the tumor, but increased in the DLN, consistent with the ability of $Xcr1^+$ cDC1 to migrate to the LN (**Fig. 3C** and **D**). These data show that intratumoral $Xcr1^+$ cDC1 vaccination can enhance T-cell priming in the DLN as well as increase immune infiltration in this aPD1-resistant model.

On the basis of the findings that cDC1 vaccine can induce tumor antigen-specific responses and alter the TME, we tested whether intratumoral delivery of $Xcr1^+$ cDC1 would be sufficient to control tumor growth. We treated the aPD1-resistant MOC1esc1 model with aPD1 alone, $Xcr1^+$ cDC1 vaccine, or the combination. Tumor growth was suppressed by the cDC1 vaccine alone, and furthermore, the combination of aPD1 and cDC1 vaccine further attenuated tumor growth (**Fig. 3E** and **F**; Supplementary Fig. S3G and S3H). Analysis of DLN and spleen cells after treatment showed tumor antigen reactivity was enhanced by cDC1 vaccine and aPD1 treatment in the DLN and by the combination in the spleen (**Fig. 3F** and **G**). These findings show that increasing intratumoral cDC1 is sufficient to reverse resistance to aPD1 treatment in an aPD1-resistant model.

CCL5 expression correlates with aPD1 sensitivity

Having identified reduced cDC1 infiltration and function in aPD1-resistant settings, we next interrogated neoadjuvant aPD1 clinical trial bulk RNA-seq data for chemokines that may influence DC migration. Comparing aPD1 responders versus nonresponders, we found that CCL5, a known DC-recruiting chemokine, was highly expressed in responder patient tumors compared with resistant tumors ($P = 0.0092$, **Fig. 4A** and **B**). Interestingly, *in vivo* CCL5 expression correlated with aPD1 resistance in the MOC models as well (**Fig. 4C**). Furthermore, CCL5 expression and the cDC score significantly correlated in the clinical cohort ($P = 0.0013$), supporting the hypothesis that CCL5 may be key to attracting cDC1 into the TME (**Fig. 4D**; Supplementary Fig. S4C). Purified $Xcr1^+$ cDC1 migrated in response to CCL5 containing media *ex vivo* (Supplementary Fig. S4D). To further explore the cellular sources of CCL5 in human tumor samples, we analyzed scRNA-seq data from patients treated with two doses of neoadjuvant pembrolizumab (18). $CD45^+$ cells isolated from two responders and two nonresponders were analyzed and unsupervised clustering identified 18 unique clusters. $CD8^+$ T-cell clusters were abundant in responders compared with nonresponders, whereas NK cells and regulatory $CD4^+$ cells were abundant in nonresponders (**Fig. 4E**). CCL5 was widely expressed across several immune populations in both responders and nonresponders (**Fig. 4F**), with $CD8^+$ T cells being one of the main sources of CCL5 expression in responders (**Fig. 4G**) along with NK and NKT cells (Supplementary Fig. S4E). Consistent with bulk RNA-seq data, the total CCL5 expression in pretreatment samples was higher in responders (**Fig. 4H**, $P = 3.03^*e{-}56$). Furthermore, to assess dynamic changes of CCL5 expression following treatment, we compared pre- and post-treatment bulk RNA-seq samples and found that CCL5 expression did not change significantly in responders or nonresponders (Supplementary Fig. S4F and S4G). Interestingly, however, pre- and posttreatment scRNA-seq data showed a specific increase of CCL5 expression in the DC population in responders (Supplementary Fig. S4H; $P = 1.78\times e{-}43$).

Next, to test whether CCL5 expression was sufficient to alter immune responses in the aPD1-resistant setting, we enforced CCL5 expression in MOC1esc1 (MOC1esc1-CCL5). Mice challenged with control or CCL5 expressing MOC1esc1 showed equivalent tumor growth (**Fig. 5A**). Analysis of the TME showed a significant increase in $Xcr1^+$ cDC1 infiltration ($P = 0.02$) in the CCL5-overexpressing tumor compared with control (**Fig. 5B**). Furthermore, CCL5 overexpression in MOC1esc1 increased $CD8^+$ and $CD8^+PD1^+$ T-cell infiltration (both $P = 0.008$, **Fig. 5C**). $Sirp\alpha^+$ cDC2 also increased

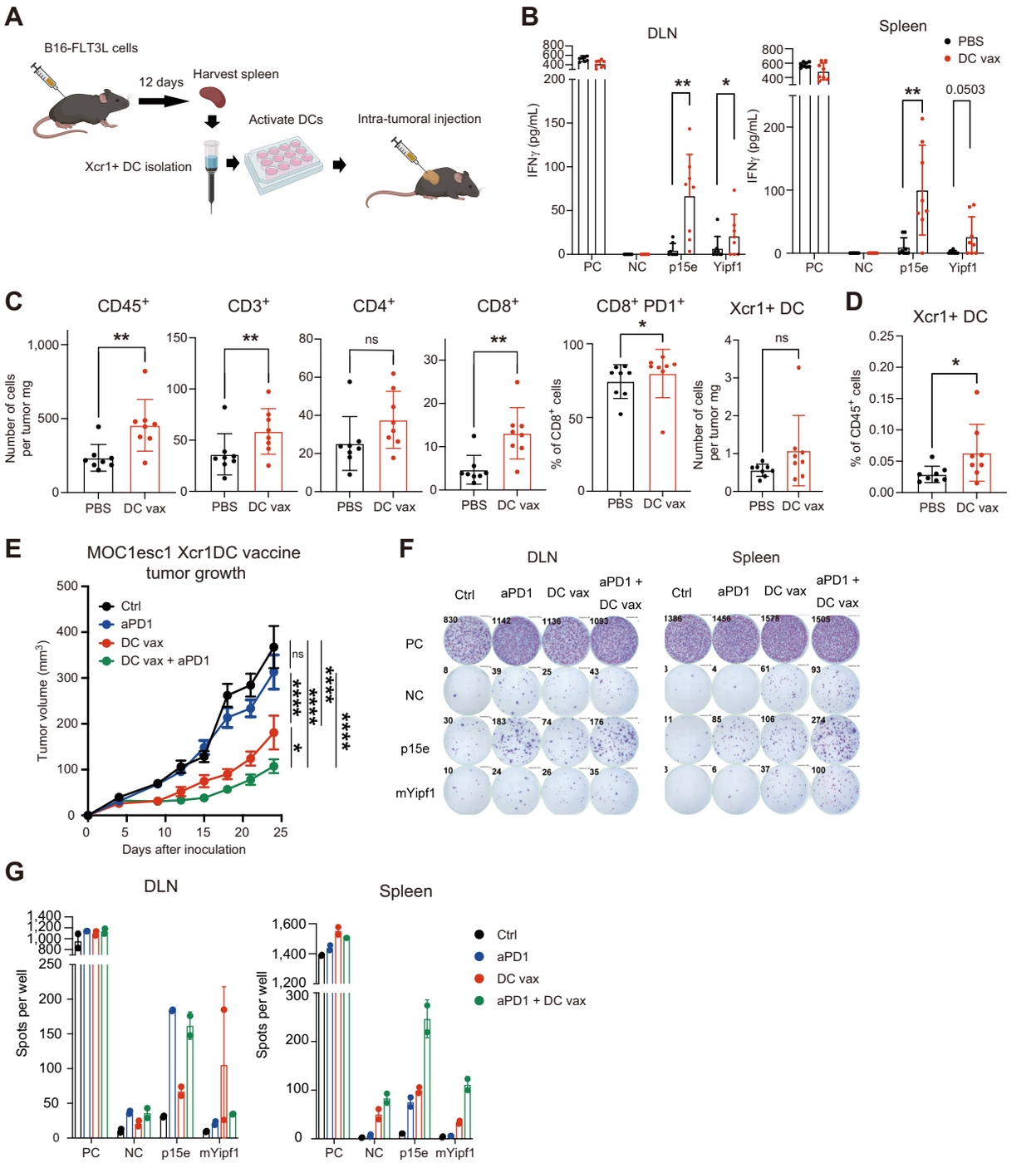

Figure 3.

Xcr1+ DC vaccine is sufficient to induce antigen-reactive T cells, alter the tumor microenvironment and attenuate tumor growth in aPD1-resistant mouse model. **A,** DC generation, Xcr1$^+$ DC isolation, and Xcr1$^+$ DC intratumoral vaccine. Vaccination was performed with 1 million Xcr1$^+$ DC. **B,** CD8$^+$ T cells were isolated from intratumoral DC-vaccinated MOC1esc1 mouse DLN or spleen on day 14 after inoculation, stimulated with peptides and evaluated for reactivity by IFNγ ELISA. PC; positive control (PMA + ionomycin), NC; negative control (no peptides), or p15e or mYipf1 peptide (0.1 μmol/L) stimulation. (n = 8, representative data of two independent experiments). **C** and **D,** Flow-cytometric analysis of MOC1esc1 tumors (**C**) and DLN (**D**) treated with intratumoral PBS or DC vaccine on days 1/4/7 after inoculation and harvested on day 14 after tumor inoculation. (n = 8, representative data of two independent experiments, gating strategies shown in Supplementary Fig. S2F and S2G). **E,** Tumor growth of aPD1-resistant MOC1esc1 model treated with intratumoral PBS (on days 1/4/7), intraperitoneal aPD1 (250 μg on days 3/6/9), intratumoral DC vaccine (1 million Xcr1+ DC on days 1/4/7), or the combination. n = 8 per group. **F,** DLN and spleens of MOC1esc1-bearing mice treated as in **E** (separate experiment) were harvested on day 13 after inoculation and cocultured with indicated peptides to test reactivity evaluated by IFNγ ELISPOT. PC; positive control (PMA + ionomycin), NC; negative control (no peptides), or p15e + mYipf1 peptide (0.1 μmol/L) stimulation. (n = 8 per group). **G,** Quantification of spots analyzed in experiment **F**. (n = 2). Individual data with mean ± SD are plotted in **B**–**D**. Data are plotted as mean ± SEM in **E**. Data were analyzed using the Mann–Whitney U test to generate two-tailed P values in **B**–**D**. Two-way ANOVA with multiple comparison was used for growth curve analysis in **E**. (**A** was generated by using BioRender under granted license.) *, $P < 0.05$; **, $P < 0.01$; ****, $P < 0.0001$.

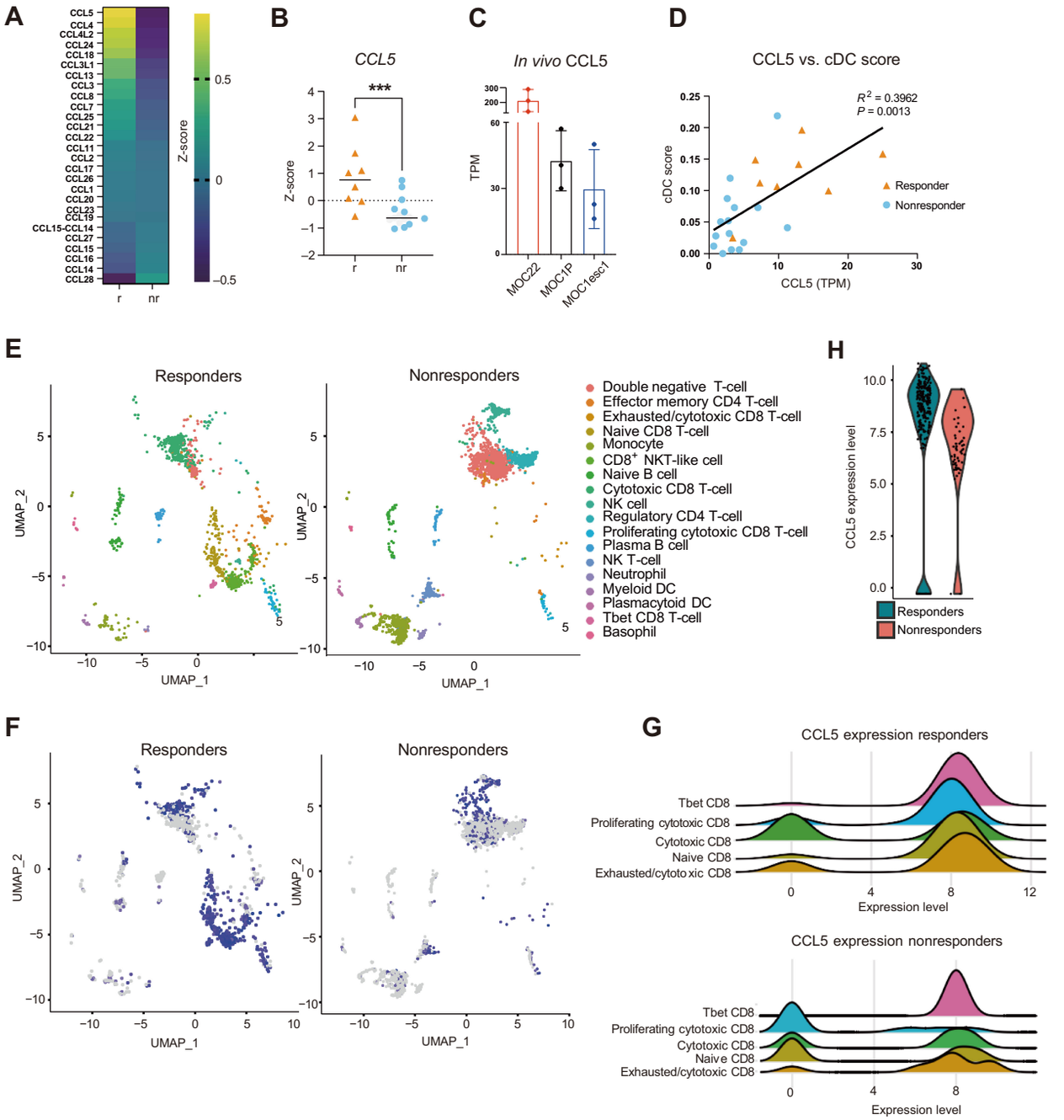

Figure 4.

CCL5 is highly expressed in aPD1-sensitive tumors. **A,** Heat map of CC chemokine ligands (CCL) based on pretreatment bulk RNA-seq data between responders (r) and nonresponders (nr). **B,** CCL5 mRNA expression comparison from bulk RNA-seq data of responders and nonresponders shown as z-score [$n = 8$ responders (r), $n = 15$ nonresponders (nr)]. **C,** CCL5 mRNA expression from bulk RNA-seq data of MOC22 tumors harvested on day 17, and MOC1P and MOC1-esc1 tumors harvested on day 14 after implantation shown as TPM ($n = 3$ each). **D,** Correlation of CCL5 mRNA expression (TPM) and cDC score (calculated from Xcell) in pretreatment bulk RNAseq data of HNSCC patient samples ($n = 8$ responders, $n = 15$ nonresponders). **E,** UMAP from scRNA-seq of pretreatment neoadjuvant pembrolizumab clinical trial patient tumors. ($n = 2$ each responder and nonresponder). **F,** Feature plots showing single-cell expression levels of CCL5 in responders and nonresponders. **G,** Distribution plots showing expression level of CCL5 in $CD8^+$ T-cell subsets. Top, responders and bottom, nonresponders. **H,** Violin plots showing relative expression levels of CCL5 in responders versus nonresponders in baseline tumors. Individual data and mean are plotted in **B**, and individual data with mean ± SD are plotted in **C**. Data were analyzed using the Mann–Whitney *U* test to generate two-tailed *P* values in **B**, Pearson correlation coefficient in **D**. ***, $P < 0.001$.

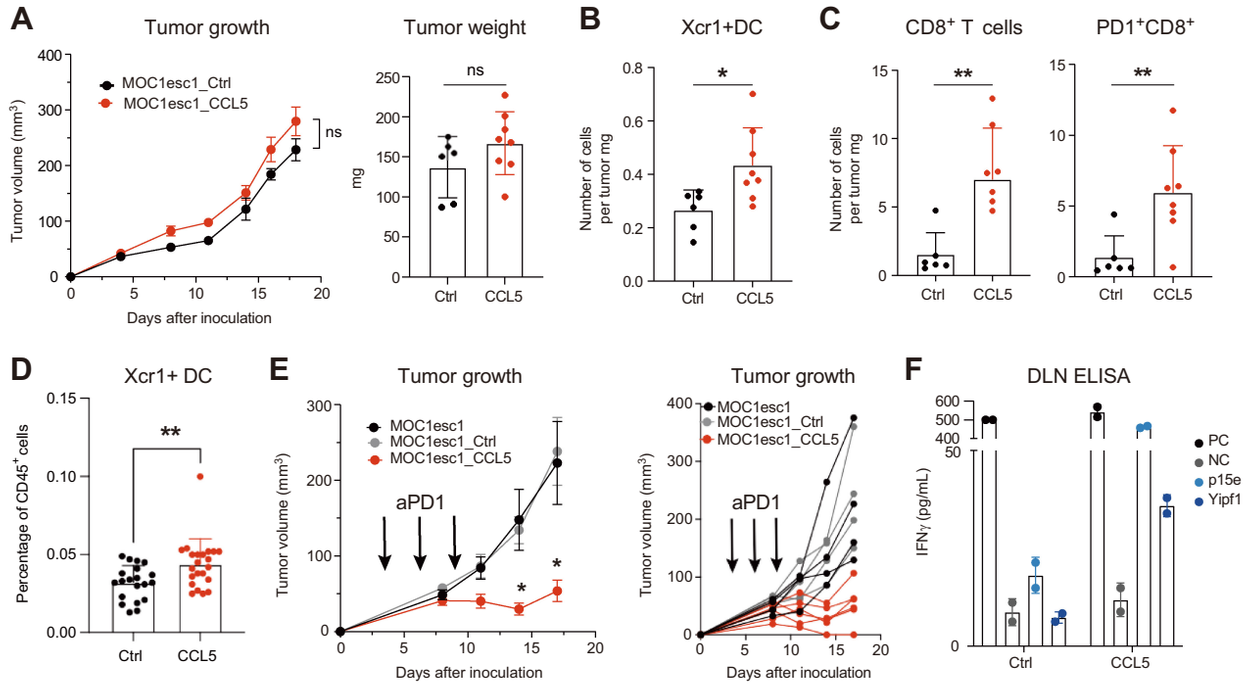

Figure 5.

CCL5 recruits cDC1 and restores aPD1 responsiveness. **A,** Comparative tumor growth of MOC1esc1_Ctrl and MOC1esc1_CCL5 cells in C57BL/6 WT mice. Tumor weight measured on day 16 after tumor inoculation ($n = 6$ for E1_Ctrl, $n = 8$ for E1_CCL5, representative data of two independent experiments). **B** and **C,** Flow-cytometric analysis of MOC1esc1_Ctrl and MOC1esc1_CCL5 tumors harvested on day 16 after tumor inoculation ($n = 6$ for E1_Ctrl, $n = 8$ for E1_CCL5, representative data of two independent experiments, gating strategies shown in Supplementary Fig. S2F and S2G). **D,** Flow-cytometric analysis of MOC1esc1_Ctrl and MOC1esc1_CCL5 DLN harvested on day 16 after tumor inoculation ($n = 20$ for Ctrl, $n = 22$ for CCL5, pooled data from three independent experiments, gating strategies shown in Supplementary Fig. S2G). **E,** Tumor growth experiment of MOC1esc1, MOC1esc1_Ctrl, and MOC1esc1_CCL5 cells (1×10^6 cells/mouse) treated with aPD1 (250 μg/mouse) on days 3, 6, and 9 (black arrows). Left shows mean ± SEM, and right shows individual tumor sizes ($n = 4$ for E1 and E1_Ctrl, $n = 6$ for E1_CCL5, representative data of two independent experiments). **F,** $CD8^+$ T cells isolated from aPD1-treated MOC1esc1_Ctrl or MOC1esc1_CCL5 DLN were stimulated with indicated peptides for 48 hours and evaluated by IFNγ ELISA. PC; positive control (PMA + ionomycin), NC; negative control (no peptides, $n = 2$) or p15e, mYipf1 peptide stimulation (0.1 μmol/L). Data are plotted as mean ± SEM in **A** and **E** and individual data with mean ± SD are plotted in **A–D** and **F**. Two-way ANOVA with multiple comparison was used for growth curve analysis in **A** and **E**. Data were analyzed using the Mann–Whitney *U* test to generate two-tailed *P* values in **A–D**. *, $P < 0.05$; **, $P < 0.01$; ns, not significant.

($P = 0.04$), but NK and $CD4^+$ T cells did not change significantly (Supplementary Fig. S5A and S5B). We also analyzed the DLN immune cell populations and found higher cDC1 representation ($P = 0.004$, **Fig. 5D**), whereas cDC2 and NK cells did not differ (Supplementary Fig. S5C). The $CD8^+$ to $CD4^+$ T-cell ratio increased, and PD1 was upregulated in both $CD4^+$ and $CD8^+$ T cells (Supplementary Fig. S5D and S5E). Interestingly, although tumor growth was comparable between MOC1esc1-Ctrl and MOC1esc1-CCL5, reactivity to antigens were slightly but significantly enhanced in CCL5 expressing TILs and DLN (Supplementary Fig. S5F). Finally, we treated mice bearing MOC1esc1 control or CCL5-transduced tumors with aPD1 and found a significant tumor size attenuation only in tumors with enforced CCL5 expression (**Fig. 5E**). DLN $CD8^+$ T cells isolated from aPD1-treated MOC1esc1-CCL5 tumors showed enhanced reactivity to the p15E-derived tumor antigen and the mYipf1 neoantigen (**Fig. 5F**). Only mice bearing CCL5-expressing tumors showed increased reactivity to tumor antigens consistent with a critical role of CCL5 in T-cell priming leading to restore aPD1 sensitivity. To further extend this finding, we enforced CCL5 expression in a different aPD1-resistant model MOC2 (21). Although the number of cDC1 did not increase, CD8 infiltration increased with higher expression of PD1 (Supplementary Fig. S5G). Given that this model is known to be immune excluded and highly resistant to ICB (21), this finding supports the activity of CCL5 to alter TME in immune "cold" tumors as well.

Discussion

Uncovering the mechanisms of aPD1 resistance is critical for developing therapeutic strategies to widely benefit patients. In this work, we show that cDC1 paucity is one of the significant correlates of aPD1 resistance in HNSCC, and inducing cDC1 in the tumor by intratumoral cDC1 vaccine is sufficient to recover aPD1 response and is mechanistically associated with reduced CCL5 expression in the tumor.

The current standard of care for most cases of locally advanced HNSCC consists of multidisciplinary treatment, including primary surgical resection followed by adjuvant radiotherapy with or without chemotherapy, respectively. Separately, some advanced HNSCC may be treated with radiotherapy-based regimens concurrent with chemotherapy. Both these modalities dramatically alter immune responses dampening the efficacy of immunotherapy for example by ablating lymph node-specific responses (14, 25). Current FDA approval of aPD1 inhibitors is restricted to patients with recurrent/metastatic HNSCC, which makes the biological study of ICB resistance complex given underlying immune alterations caused by

prior therapies. Here, we analyzed neoadjuvant aPD1-treated patients with HNSCC focusing on treatment-naïve patient samples with defined pathologic tumor response to aPD1 monotherapy. This approach allowed us to focus on mechanisms of ICB resistance in the absence of antecedent immune system alteration.

Previous studies have identified tumor-infiltrating DC as significantly correlated with prognosis in several cancer types (10, 13, 26) and ICB response in human melanoma (11, 27). Our analysis of neoadjuvant aPD1-treated patients with HNSCC showed a similar association of DC infiltration with pathologic response. By using syngeneic mouse HNSCC models, we found aPD1 resistance mirrored human HNSCC cDC1 paucity and identified decreased DC activation in the mouse tumor DLN with poor priming of $CD8^+$ T cells. These results extend the important role of cDC1 in both the tumor and DLN to elicit antitumor response to aPD1 treatment.

Given the important role of cDC1, therapies to increase intratumoral cDC1 such as FLT3 L administration have been explored and shown to be effective in preclinical models (28–30). Extending data from a neoadjuvant aPD1 melanoma clinical trial, Hoefsmit and colleagues (27) identified inhibitor of apoptosis antagonism as an approach to enhance cross presentation. Intriguingly, combination of xevinapant, an antagonist of inhibitor of apoptosis proteins, and chemoradiotherapy has shown compelling clinical data in HNSCC (31), but it remains unclear whether enhanced cross presentation contributes to these outcomes.

TME disruption of DC function has multiple etiologies, including local immunosuppression and recruitment (32). We showed that inducing intratumoral DC by cDC1 vaccination was sufficient to recover aPD1 resistance, supported by increased antigen-specific responses and enhanced T-cell infiltration. Although DC vaccines have shown limited clinical effect in solid tumors (33), alternative approaches such as delivering CCL5 to tumors may represent approaches to enhance DC infiltration and function, including in the aPD1-resistant setting.

Focusing on the mechanism of DC deficit, we found that CCL5 was one of the highest expressed chemokines in aPD1 responder patients at baseline and that CCL5 expression positively correlated with cDC infiltration. Both pro- and antitumor effects of CCL5 have been reported with some studies showing CCL5 as a correlate of tumor progression (34), whereas others have shown it as a favorable marker of T-cell infiltration (35). Böttcher showed that CCL5 expressed by NK cells can recruit cDC1 into the tumor, whereas prostaglandin E2 production in the tumor can attenuate this effect (10). We did not see any correlation between prostaglandin-related gene expression and a DC signature in HNSCC mouse models or the neoadjuvant pembrolizumab cohort suggesting a distinct mechanism for CCL5 deficiency in HNSCC such as epigenetic silencing (36). Importantly, the correlation of CCL5 and aPD1 sensitivity has not been previously demonstrated. Kirchhammer and colleagues (37) compared aPD1-treated melanoma tumor samples and reported that there was a significant increase of CCL5 expression in responder patients. Here, we show that at baseline, CCL5 expression is higher in responders, indicating an important role of this chemokine to "set" the tumors to be ICB responsive. Enforced CCL5 expression in our aPD1-resistant model did not alter tumor growth but increased cDC1 infiltration in tumors and lymph nodes, increased $CD8^+$ T-cell infiltration in the TME, and sensitized the tumor to subsequent aPD1 treatment with enhanced tumor reactive $CD8^+$ T cells in the DLN. Collectively, these data reveal an important role of CCL5 in enhancing antigen-specific responses likely via recruitment of cDC1 and improving HNSCC response to aPD1 therapy.

There are several limitations to this study. Because of lack of sample availability, we were not able to validate DC paucity in our clinical trial baseline patient tumors by flow cytometry or other methods other than RNA expression. The human $CD45^+$ scRNA-Seq was from a limited sample set, and definitive conclusions with respect to specific CCL5-producing cells could not be made. Finally, we do not know exactly what mechanisms contribute to reduced CCL5 expression in nonresponders. Our future work is aimed at approaches to enhance CCL5 expression in the TME with further mechanistic dissection of its role in DC: T-cell interactions. In conclusion, approaches to enhance DC recruitment and priming in conjunction with aPD1 therapies may advance the care of patients with HNSCC.

Authors' Disclosures

D. Adkins reports grants and personal fees from Merck during the conduct of the study; grants and personal fees from Pfizer, Eli Lilly, Celgene/BMS, and Cue Biopharma; personal fees from Loxo Oncology; and grants from Novartis, Roche, Aduro, Atara, Matrix, Blueprint Medicine, Celldex, Enzychem, Exilixis, Shanghai *De Novo*, Kura, AstraZeneca, Medimmune, and Innate outside the submitted work. R. Uppaluri reports grants from NIH during the conduct of the study and personal fees from Merck Inc., Daiichi Sankyo, Regeneron, and Washington University outside the submitted work. No disclosures were reported by the other authors.

Authors' Contributions

S. Saito: Conceptualization, resources, data curation, formal analysis, investigation, visualization, methodology, writing–original draft. **M. Kono:** Conceptualization, resources, data curation, formal analysis, investigation, visualization, methodology, writing–original draft. **H.C.B. Nguyen:** Software, formal analysis, visualization, writing–review and editing. **A.M. Egloff:** Supervision, validation, project administration, writing–review and editing. **C. Messier:** Supervision. **P. Lizotte:** Supervision. **C. Paweletz:** Supervision. **D. Adkins:** Supervision. **R. Uppaluri:** Conceptualization, resources, supervision, funding acquisition, validation, methodology, project administration, writing–review and editing.

Acknowledgments

We thank all members of the Uppaluri laboratory and Dr. Gavin Dunn for thoughtful discussions. We thank Clint Allen for the mKATE2–SIINFEKL plasmid and U. Von Andrian/G. Dranoff for B16-FLT3L cells. We thank the Robert A. and Renee E. Belfer Foundation and Expect Miracles Foundation for support and all the patients/families who participated in the neoadjuvant anti-PD1 clinical trial. Work in the Uppaluri laboratory was supported by NIH/NCI/NIDCR U01DE029188 and NIH/NIDCR R01DE027736.

Note

Supplementary data for this article are available at Clinical Cancer Research Online (http://clincancerres.aacrjournals.org/).

Received November 7, 2023; revised December 27, 2023; accepted February 14, 2024; published first February 19, 2024.

References

1. Sung H, Ferlay J, Siegel RL, Laversanne M, Soerjomataram I, Jemal A, et al. Global cancer statistics 2020: GLOBOCAN estimates of incidence and mortality worldwide for 36 cancers in 185 countries. CA Cancer J Clin 2021;71:209–49.
2. Chaturvedi AK, Engels EA, Pfeiffer RM, Hernandez BY, Xiao W, Kim E, et al. Human papillomavirus and rising oropharyngeal cancer incidence in the United States. J Clin Oncol 2023;41:3081–8.

3. Ferris RL, Blumenschein G Jr, Fayette J, Guigay J, Colevas AD, Licitra L, et al. Nivolumab for recurrent squamous cell carcinoma of the head and neck. N Engl J Med 2016;375:1856–67.
4. Cohen EEW, Soulières D, Le Tourneau C, Dinis J, Licitra L, Ahn MJ, et al. Pembrolizumab versus methotrexate, docetaxel, or cetuximab for recurrent or metastatic head-and-neck squamous cell carcinoma (KEYNOTE-040): a randomised, open-label, phase 3 study. Lancet 2019;393:156–67.
5. Harrington KJ, Burtness B, Greil R, Soulières D, Tahara M, de Castro G Jr, et al. Pembrolizumab with or without chemotherapy in recurrent or metastatic head and neck squamous cell carcinoma: updated results of the phase III KEYNOTE-048 study. J Clin Oncol 2023;41:790–802.
6. Harrington KJ, Ferris RL, Gillison M, Tahara M, Argiris A, Fayette J, et al. Efficacy and safety of nivolumab plus ipilimumab vs. nivolumab alone for treatment of recurrent or metastatic squamous cell carcinoma of the head and neck: the phase 2 CheckMate 714 randomized clinical trial. JAMA Oncol 2023;9:779–89.
7. Morad G, Helmink BA, Sharma P, Wargo JA. Hallmarks of response, resistance, and toxicity to immune checkpoint blockade. Cell 2021;184:5309–37.
8. Kalbasi A, Ribas A. Tumour-intrinsic resistance to immune checkpoint blockade. Nat Rev Immunol 2020;20:25–39.
9. Kirchhammer N, Trefny MP, Auf der Maur P, Läubli H, Zippelius A. Combination cancer immunotherapies: emerging treatment strategies adapted to the tumor microenvironment. Sci Transl Med 2022;14:eabo3605.
10. Böttcher JP, Bonavita E, Chakravarty P, Blees H, Cabeza-Cabrerizo M, Sammicheli S, et al. NK cells stimulate recruitment of cDC1 into the tumor microenvironment promoting cancer immune control. Cell 2018;172:1022–37.
11. Barry KC, Hsu J, Broz ML, Cueto FJ, Binnewies M, Combes AJ, et al. A natural killer-dendritic cell axis defines checkpoint therapy-responsive tumor microenvironments. Nat Med 2018;24:1178–91.
12. Böttcher JP, Reis e Sousa C. The role of type 1 conventional dendritic cells in cancer immunity. Trends Cancer 2018;4:784–92.
13. Meiser P, Knolle MA, Hirschberger A, de Almeida GP, Bayerl F, Lacher S, et al. A distinct stimulatory cDC1 subpopulation amplifies CD8(+) T-cell responses in tumors for protective anticancer immunity. Cancer Cell 2023;41:1498–515.
14. Saddawi-Konefka R, O'Farrell A, Faraji F, Clubb L, Allevato MM, Jensen SM, et al. Lymphatic-preserving treatment sequencing with immune checkpoint inhibition unleashes cDC1-dependent antitumor immunity in HNSCC. Nat Commun 2022;13:4298.
15. Judd NP, Winkler AE, Murillo-Sauca O, Brotman JJ, Law JH, Lewis JS Jr, et al. ERK1/2 regulation of CD44 modulates oral cancer aggressiveness. Cancer Res 2012;72:365–74.
16. Zhou L, Zeng Z, Egloff AM, Zhang F, Guo F, Campbell KM, et al. Checkpoint blockade-induced $CD8^+$ T-cell differentiation in head and neck cancer responders. J Immunother Cancer 2022;10:e004034.
17. Uppaluri R, Campbell KM, Egloff AM, Zolkind P, Skidmore ZL, Nussenbaum B, et al. Neoadjuvant and adjuvant pembrolizumab in resectable locally advanced, human papillomavirus-unrelated head and neck cancer: a multicenter, Phase II trial. Clin Cancer Res 2020;26:5140–52.
18. Oliveira G, Egloff AM, Afeyan AB, Wolff JO, Zeng Z, Chernock RD, et al. Preexisting tumor-resident T cells with cytotoxic potential associate with response to neoadjuvant anti-PD-1 in head and neck cancer. Sci Immunol 2023;8:eadf4968.
19. Obermajer N, Urban J, Wieckowski E, Muthuswamy R, Ravindranathan R, Bartlett DL, et al. Promoting the accumulation of tumor-specific T cells in tumor tissues by dendritic cell vaccines and chemokine-modulating agents. Nat Protoc 2018;13:335–57.
20. Busselaar J, Tian S, van Eenennaam H, Borst J. Helpless priming sends CD8(+) T cells on the road to exhaustion. Front Immunol 2020;11:592569.
21. Zolkind P, Przybylski D, Marjanovic N, Nguyen L, Lin T, Johanns T, et al. Cancer immunogenomic approach to neoantigen discovery in a checkpoint blockade responsive murine model of oral cavity squamous cell carcinoma. Oncotarget 2018;9:4109–19.
22. Spranger S, Dai D, Horton B, Gajewski TF. Tumor-residing Batf3 dendritic cells are required for effector T-cell trafficking and adoptive T-cell therapy. Cancer Cell 2017;31:711–23.
23. Aran D, Hu Z, Butte AJ. xCell: digitally portraying the tissue cellular heterogeneity landscape. Genome Biol 2017;18:220.
24. Huang AY, Gulden PH, Woods AS, Thomas MC, Tong CD, Wang W, et al. The immunodominant major histocompatibility complex class I-restricted antigen of a murine colon tumor derives from an endogenous retroviral gene product. Proc Natl Acad Sci USA 1996;93:9730–5.
25. Miyauchi S, Kim SS, Pang J, Gold KA, Gutkind JS, Califano JA, et al. Immune modulation of head and neck squamous cell carcinoma and the tumor microenvironment by conventional therapeutics. Clin Cancer Res 2019;25:4211–23.
26. Broz ML, Binnewies M, Boldajipour B, Nelson AE, Pollack JL, Erle DJ, et al. Dissecting the tumor myeloid compartment reveals rare activating antigen-presenting cells critical for T-cell immunity. Cancer Cell 2014;26:638–52.
27. Hoefsmit EP, van Royen PT, Rao D, Stunnenberg JA, Dimitriadis P, Lieftink C, et al. Inhibitor of apoptosis proteins antagonist induces T-cell proliferation after cross-presentation by dendritic cells. Cancer Immunol Res 2023;11:450–65.
28. Salmon H, Idoyaga J, Rahman A, Leboeuf M, Remark R, Jordan S, et al. Expansion and activation of CD103(+) dendritic cell progenitors at the tumor site enhances tumor responses to therapeutic PD-L1 and BRAF inhibition. Immunity 2016;44:924–38.
29. Oba T, Long MD, Keler T, Marsh HC, Minderman H, Abrams SI, et al. Overcoming primary and acquired resistance to anti–PD-L1 therapy by induction and activation of tumor-residing cDC1. Nat Commun 2020;11:5415.
30. Hegde S, Krisnawan VE, Herzog BH, Zuo C, Breden MA, Knolhoff BL, et al. Dendritic cell paucity leads to dysfunctional immune surveillance in pancreatic cancer. Cancer Cell 2020;37:289–307.
31. Sun XS, Tao Y, Le Tourneau C, Pointreau Y, Sire C, Kaminsky MC, et al. Debio 1143 and high-dose cisplatin chemoradiotherapy in high-risk locoregionally advanced squamous cell carcinoma of the head and neck: a double-blind, multicentre, randomised, phase 2 study. Lancet Oncol 2020;21:1173–87.
32. Mestrallet G, Sone K, Bhardwaj N. Strategies to overcome DC dysregulation in the tumor microenvironment. Front Immunol 2022;13:980709.
33. Harari A, Graciotti M, Bassani-Sternberg M, Kandalaft LE. Antitumour dendritic cell vaccination in a priming and boosting approach. Nat Rev Drug Discov 2020;19:635–52.
34. Melese ES, Franks E, Cederberg RA, Harbourne BT, Shi R, Wadsworth BJ, et al. CCL5 production in lung cancer cells leads to an altered immune microenvironment and promotes tumor development. Oncoimmunology 2022;11:2010905.
35. Romero JM, Grunwald B, Jang GH, Bavi PP, Jhaveri A, Masoomian M, et al. A four-chemokine signature is associated with a T-cell–inflamed phenotype in primary and metastatic pancreatic cancer. Clin Cancer Res 2020;26:1997–2010.
36. Dangaj D, Bruand M, Grimm AJ, Ronet C, Barras D, Duttagupta PA, et al. Cooperation between constitutive and inducible chemokines enables T-cell engraftment and immune attack in solid tumors. Cancer Cell 2019;35:885–900.
37. Kirchhammer N, Trefny MP, Natoli M, Brücher D, Smith SN, Werner F, et al. NK cells with tissue-resident traits shape response to immunotherapy by inducing adaptive antitumor immunity. Sci Transl Med 2022;14:eabm9043.